Journal of
Synchrotron
Radiation

ISSN 0909-0495

Received 7 October 2004
Accepted 14 April 2005

Mechanical properties of cellulose fibres and wood. Orientational aspects *in situ* investigated with synchrotron radiation

Klaas Kölln,[a] Ingo Grotkopp,[a] Manfred Burghammer,[b] Stephan V. Roth,[b] Sergio S. Funari,[c,d] Martin Dommach[c,d] and Martin Müller[a]*

[a]Institut für Experimentelle und Angewandte Physik, Universität Kiel, Leibnizstraße 19, D-24098 Kiel, Germany, [b]European Synchrotron Radiation Facility, BP 220, F-38043 Grenoble CEDEX, France, [c]Max-Planck-Institut für Kolloid- und Grenzflächenforschung, D-14424 Potsdam, Germany, and [d]c/o HASYLAB at DESY, Notkestraße 85, D-22603 Hamburg, Germany.
E-mail: mmueller@physik.uni-kiel.de

Highly oriented native cellulose fibres (flax) and softwood (pine) have been investigated by means of X-ray diffraction. Local structural information was obtained by using X-ray microbeams. Tensile tests were performed *in situ*, revealing a change of orientation of cellulose microfibrils in materials with tensile strain. In flax fibres, the microfibrils rotate during the first percent of stretching, into a more parallel orientation with respect to the fibre axis. For wood, a decrease of orientation with the onset of strain hardening is found for the first time.

Keywords: X-ray diffraction; cellulose fibres; flax; wood; mechanical properties; tensile strain; strain hardening; orientation distribution.

1. Introduction

Cellulose and wood are hierarchically structured biomaterials. Their unique mechanical properties are of great importance for the plants synthesizing them as their main structural materials. Native cellulose fibres may be as strong as high-tech fibres, such as, for example, Kevlar (Satta *et al.*, 1986), and wood combines high strength with low density.

Cellulose is semicrystalline, with small crystals, *microfibrils*, embedded in a disordered matrix. The length of the microfibrils is of the order of micrometres, whereas their species-specific diameter is only 2–25 nm (O'Sullivan, 1997). In plant bast fibres (flax, hemp, ramie, jute *etc.*), the microfibrils are well aligned with respect to the fibre axis. Wood cells have an additional structural parameter with an important influence on the mechanical properties, the so-called *microfibril angle* (MFA). The microfibrils are wound around the cell in a helical fashion. The MFA is the angle of that helix with respect to the longitudinal cell axis. The smaller the MFA (*i.e.* the steeper the helix) the higher the longitudinal Young's modulus of the wood cell (Reiterer *et al.*, 1999). The embedding matrix is reinforced by lignin in woody plant tissue.

X-ray diffraction and small-angle X-ray scattering with synchrotron radiation are well established methods for the determination of structural details of biological materials, and there are a number of recent publications on their application to cellulose fibres and wood (Lichtenegger *et al.*, 1999; Müller, Czihak *et al.*, 2000; Burghammer *et al.*, 2003; Keckes *et al.*, 2003). Wide-angle X-ray diffraction (WAXD) gives access to crystallographic parameters of the cellulose microfibrils on the *nanometre* scale, as well as to their texture. In the case of highly oriented cellulose fibres, the texture is best described by a perfect fibre texture with some degree of misorientation, accounted for by a distribution of orientations around the longitudinal fibre axis. In wood, the presence of the microfibril angle makes the texture analysis more complicated (Cave, 1997). In the case of small MFAs, however, a description like that of cellulose fibres is adequate (Lichtenegger *et al.*, 1998). Small-angle X-ray scattering is sensitive to inhomogeneities on *mesoscopic* length scales, such as the contrast between microfibrils and embedding matrix (Jakob *et al.*, 1994) or pores.

A third length scale on the *microscopic* level has become accessible by using X-ray microbeams produced by third-generation synchrotron radiation sources. Samples can be scanned through the microbeam, yielding maps of the parameters described above with a position resolution that corresponds to that of optical microscopy (Riekel, 2000). The small beam size can also be exploited for the measurement of single plant fibre cells (Müller *et al.*, 1998). The focused X-rays are sufficiently intense to make the investigation of weakly scattering biological materials such as cellulose and wood possible. In addition, a single two-dimensional diffraction pattern can be obtained within a few seconds because of the high flux density of the focused X-rays.

In most cases, fibres are treated as homogeneous systems in the sense that parameters obtained by X-ray diffraction are taken as representative of the sample as a whole. This assumption is valid only if the morphological structure of the fibre is homogeneous throughout the sample. Such treatment neglects the influence of any defects in the morphological structure, which were introduced during growth or the production of the fibre, as well as systematic variations in the fibre structure, such as skin–core arrangements. Using X-ray microdiffraction techniques with typical beam diameters much smaller than the diameter of the sample, information can be gained on a local length scale. Thus it becomes possible to investigate inhomogeneities of the fibre structure and properties.

A main strength of X-ray scattering is that this technique can easily be combined with other experiments *in situ*. Our aim is to establish the relation between structural parameters accessible by X-ray scattering and the mechanical properties of native cellulose fibres and wood. Thus tensile tests (stretching in the longitudinal cell direction) were carried out on single fibres and thin wood foils, and two-dimensional WAXD patterns were collected simultaneously. In this article, we focus on the orientational properties of the microfibrils in the composite materials under investigation, namely flax fibres and pine wood. A second aspect concerns the development of *in situ* stretching techniques over the past few years; the speed of the progress can be seen from the results presented here.

In the following, we briefly present the samples investigated (§2.1) and the mechanical testing devices (§2.2) used in the synchrotron WAXD experiments (§2.3). The results of three exemplary experiments with *in situ* stretching are reported: scanning microdiffraction on a single flax fibre (§3.1), a fast stretching experiment with a constant strain rate on flax (§3.2) and a similar experiment on thin sections of pine wood (§3.3).

2. Experimental details

2.1. Samples

Straight single fibres from bundles of bleached industrial flax fibres were selected for mounting with the help of a stereo microscope. The typical diameter of the fibres was 20 µm and their length was 5 mm. Tangential sections of earlywood (0.2 mm thickness, 5 mm width) were cut from pine timber. The samples were checked with an optical microscope for longitudinal orientation.

All experiments were carried out under ambient conditions. The experimental hutches at the synchrotron sources were air-conditioned at room temperature with a relative humidity of about 40%. For the wood samples, this results in a moisture content of less than 10 wt%, well below the fibre saturation point of 30 wt%, at which the cell walls are saturated with water and the lumina begin to fill (Noack & Schwab, 1996).

2.2. Mechanical testing devices

The devices used for this work were built at the European Synchrotron Radiation Facility and the University of Kiel. They were constructed to fit the restricted space at synchrotron radiation sources, which is usually a problem for commercially available instruments.

2.2.1. ESRF stretching device for single fibres. For the experiments with single flax fibres, stretching devices available at the European Synchrotron Radiation Facility (ESRF, Grenoble, France) were used. The first device (see §3.1) is based on a solid metal frame with flexure hinges and a piezo actuator (Riekel *et al.*, 1999). Strain is set manually by changing the piezo voltage, measured with a gauge incorporated into the frame and controlled electronically in a closed loop. An Entran force sensor with a maximum load of 500 mN was used to measure the force. The samples (individual flax fibres) were directly fixed to the jaws of the stretching device with cyanoacrylate glue (Loctite 401). The free fibre length was typically 3 mm; the maximum strain was limited to about 10% by the maximum gap increase of 280 µm. In the second experiment (see §3.2), a different piezo-driven device with a larger travel range but the same force sensor was used. This setup was interfaced with a computer and allowed for measuring with a constant strain rate while acquiring X-ray diffraction data. In this experiment, individual fibres were first glued to paper frames, which could then be easily fixed to the jaws of the stretching device. The sides of the frame were cut before the tensile tests.

2.2.2. Kiel stretching device for fibre bundles and wood foils. For tensile tests of large samples, such as fibre bundles and wood foils, a larger stretching device was built. The device is designed for a maximum load of 2.5 kN and has a maximum travel range of 45 mm. The motion of the stretching device can be controlled with a resolution of less than a micrometre. The device is driven by a synchronous servo motor equipped with a Sincos encoder and is computer-controlled. A set of force sensors with different maximal loads (F_{max} = 25, 125 and 2500 N) allows for an adjustment of the resolution of the force measurements. The device can be operated at synchrotron beamlines as well as neutron spectrometers. For measurements at the latter instruments, the sample can be kept under vacuum. The wood foils were fixed to the stretching device by clamps.

2.3. X-ray diffraction experiments with synchrotron radiation

2.3.1. Experiments at ID13, ESRF. The microfocus beamline ID13 at the ESRF is an experimental station dedicated to the use of X-ray microbeams and has been described in detail by Riekel (2000). The so-called scanning setup used for the experiments presented here is optimized for position-resolved investigations of single fibres and inhomogeneous samples that can be scanned through the microbeam with an accuracy better than 1 µm. X-ray energies of 15.8 keV (first experiment, see §3.1) and 13.1 keV (second experiment, see §3.2), corresponding to wavelengths of 0.078 and 0.096 nm, respectively, were selected with the Si(111) double monochromator. The X-rays were then focused by an ellipsoidal mirror to a spot size of about 20 µm × 40 µm. In the first experiment, a tapered glass capillary produced a beam of 2 µm in diameter; in the

second experiment, a collimator cut the beam cross section down to 5 μm in diameter. Slit scattering was removed by an additional guard aperture. A small cylindrical lead beam stop (about 300 μm in diameter) was placed a few millimetres behind the samples to limit air scattering. Two-dimensional diffraction patterns were collected with a CCD detector. In the first experiment, a MAR CCD detector (pixel size 64.45 μm × 64.45 μm) with a read-out time of about 4 s was placed at a distance of 96.5 mm behind the sample. The second experiment could profit from the fast read-out (276 ms) of a XIDIS Photonic Science CCD detector (pixel size 27.6 μm × 27.6 μm, sample-to-detector distance 36.5 mm).

2.3.2. Experiments at A2, HASYLAB. At beamline A2 at HASYLAB (DESY, Hamburg, Germany) the wavelength is fixed at 0.15 nm, corresponding to an incoming photon energy of 8.3 keV. The Ge(111) monochromator serves for horizontal focusing; in the vertical direction the beam is focused by a Ni mirror. For our experiments (see §3.3), the X-ray beam was defined to a cross section of 250 μm × 250 μm using a pair of microslits. Diffuse slit scattering was removed by the last pair of slits close to the sample. The sample in the Kiel stretching device (see §2.2.2) was placed 3 mm behind the Kapton exit window of the evacuated beam path. In order to minimize air scattering, a motorized cylindrical lead beam stop of diameter 0.8 mm was used at a distance of 8 mm behind the sample. Two-dimensional diffraction patterns were collected with a Gemstar Photonic Science CCD detector (image-intensified, overall read-out time less than 500 ms, 66.2 μm × 66.2 μm pixel size). The sample-to-detector distance was 43.4 mm.

2.3.3. Data analysis. In all samples, cellulose is the only crystalline constituent. The strongest reflection in the fibre diffraction diagram of cellulose is the 200 Bragg reflection (notation of Woodcock & Sarko, 1980) found on the equator of the diffraction pattern (see Fig. 1 for flax and pine wood).

The two-dimensional data files were analysed using the ESRF *fit2d* software package. The diffraction diagrams of the Photonic Science CCD detectors were corrected for detector distortion (Hammersley *et al.*, 1994). Radial integration of the cellulose 200 reflection was performed in order to obtain one-dimensional scans of the azimuthal intensity distribution, which was used to determine azimuthal reflection widths.

Hermans' orientation function, usually denoted by f_c, is a frequently used measure for the orientation in fibres (Stein, 1958; Alexander, 1979). The parameter f_c is 0 for no preferred orientation of the crystals in the sample (*i.e.* an ideal powder texture) and 1 if all crystals are perfectly aligned with respect to each other (*i.e.* an ideal fibre texture). Typical values for fibres with a high degree of orientation are well above f_c = 0.90.

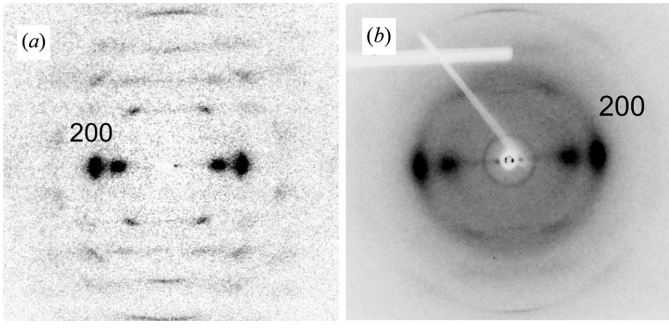

Figure 1
(*a*) Typical two-dimensional cellulose diffraction pattern (background subtracted) of a 20 μm-thick single cellulose fibre, measured with a 2 μm × 2 μm X-ray beam in 2 s (beamline ID13, ESRF). (*b*) Typical two-dimensional cellulose diffraction pattern (raw data without background subtraction) of a 200 μm-thick tangential section of pine wood, measured with a 250 μm × 250 μm X-ray beam in 3 s (beamline A2, HASYLAB). The circle in the centre of the image is scattering at the Kapton beam exit window; the shadow is from the beam stop holder. The strongest reflections on the equator of the fibre diffraction diagrams (left and right of the centre) correspond to the (200) Bragg planes of native cellulose I.

3. Results and discussion

3.1. Scanning microdiffraction of a single flax fibre (ESRF, ID13)

In order to measure the orientation function f_c of the cellulose microfibrils spatially resolved, a single flax fibre was scanned vertically and horizontally with an X-ray beam focused down to 2 μm. The fibre was mounted vertically in the ESRF stretching device described above (§2.2.1). One scan consisted of three (horizontal) by nine (vertical) diffraction images with a horizontal spacing of 4 μm and a vertical spacing of 15 μm. The three vertical columns were shifted by 5 μm in the vertical direction with respect to each other (see Fig. 2 for the scan pattern). The individual measurement points were thus distributed evenly over the scanned area. The total scan area measured approximately 10 μm × 140 μm, amounting to

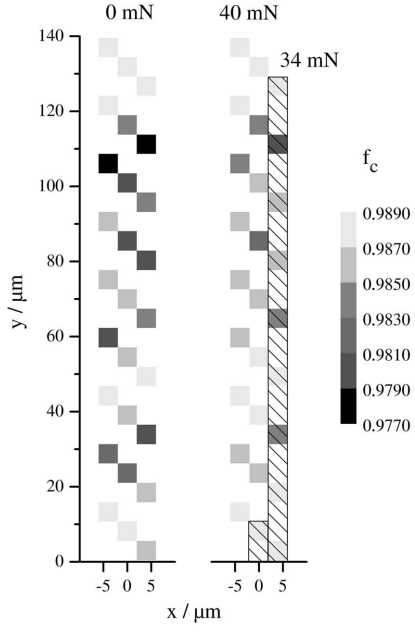

Figure 2
Greyscale-coded plot of Hermans' orientation function values f_c for forces of F = 0 mN and F = 40 mN at different positions on a single flax fibre. The y coordinate is the longitudinal fibre direction; z is perpendicular to y. The fibre broke after 17 points measured at 40 mN; the missing values have been replaced by those at 34 mN (hatched area). The X-ray beam diameter was 2 μm (microfocus beamline ID13, ESRF).

about half of the fibre diameter and 5% of the total fibre length. The strain ε of the fibre was held constant while the diffraction images for one scan of the fibre were taken. The fibre was allowed to relax for a few minutes prior to each scan until the measured force remained constant. We measured at six different strain values up to 0.9%. The exposure time for one diffraction image was 20 s; the total time for one complete scan was 15 min. After completion of one scan the fibre was strained further and the next scan was started. A total of five scan cycles could be completed. The fibre broke during the 18th exposure of the sixth scan (maximum force 40 mN). Unfortunately, the fibre was completely destroyed in the demounting process and thus no exact measurement of the fibre cross-section area was possible. Therefore, only applied forces instead of stress values are given.

Fig. 2 is a greyscale-coded map of the orientation function f_c of the cellulose microfibrils with respect to the fibre axis evaluated from the X-ray diffraction images. Plots are shown for tensile forces of $F = 0$ mN (corresponding to $\varepsilon = 0\%$) and $F = 40$ mN ($\varepsilon = 0.9\%$). The missing data points for $F = 40$ mN, as a result of the premature rupture of the fibre, are replaced by the corresponding values of the preceding scan cycle with $F = 34$ mN (hatched area). Both graphs show an irregular distribution of the orientation function values along the width and the length of the fibre. Specifically, no skin–core structure, as found for artificial fibres such as Kevlar (Riekel *et al.*, 1999) and viscose (Müller, Riekel *et al.*, 2000), can be observed. In these materials the outer 'skin' of the fibres possesses a higher degree of orientation than the fibre 'core'.

The distribution of the orientation function values is asymmetric for all scans. At most of the measured points the microfibrils are highly oriented, while only a few regions possess a significantly lower orientation. Upon stretching of the fibre, the distribution of the orientation function values becomes sharper with increasing strain. Values of low orientation do not occur after the beginning of the experiment. In total, a tendency to higher orientation function values is observed, *i.e.* the mean value of the distribution increases. In Fig. 3, this is shown for three different mean orientation values at zero strain, namely those of the upper (circles) and lower (triangles) parts of the region investigated and those of all data points (squares). Areas of the fibre that were already well oriented at the start of the experiment show little or no improvement of f_c while those parts exhibiting a low initial orientation increase markedly. The curves become steeper for higher strain, *i.e.* the orientation improvement upon stretching is stronger the higher the strain. No values higher than $f_c = 0.989$ that have already been found for the unstrained fibre are observed during the course of the experiment, suggesting that there is an upper limit to the value of the orientation function f_c which can be reached by straining the fibre. This effect has also been observed for Kevlar fibres (Riekel *et al.*, 1999).

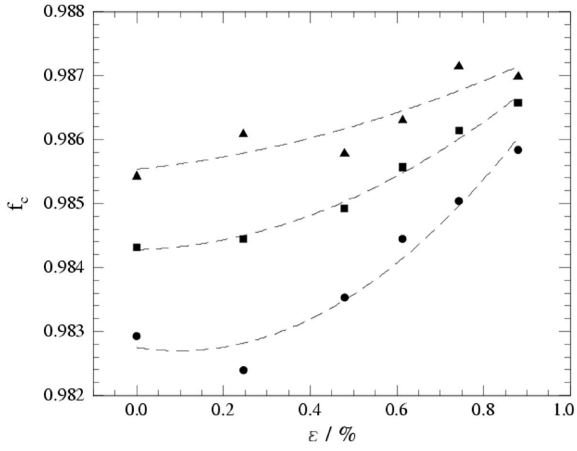

Figure 3
Strain dependence of Hermans' orientation function f_c for the same flax fibre as in Fig. 2. We show the average values over all 27 data points (squares), the upper 12 points (circles) and the lower 12 points (triangles). The dashed lines are a guide to the eye.

3.2. Stretching experiments on single flax fibres with constant strain rate (ESRF, ID13)

Flax fibres show a considerable amount of viscoelasticity. As already mentioned in the previous section, relaxation after increasing fibre strain occurs on the timescale of minutes. In order to measure the instant mechanical response of a flax fibre (like that experienced in the native environment when, for example, a plant stem is bent by wind), the strain rate has to be fast enough to avoid relaxation. In the experiments described here, the fibres were strained with a rate of 0.6% s^{-1}, corresponding to 2.0 µm s^{-1}. The cross-section areas A of fibres were determined microscopically and used to calculate the applied stress $\sigma = F/A$ with the measured force F. The obtained stress–strain curves $\sigma(\varepsilon)$ are linear over the whole range with slope E (Young's modulus). On average, a Young's modulus of 24.7 GPa and a maximum strain of 2.5% were measured. These values are in good agreement with those for industrial flax fibres found in the literature (Morton & Hearle, 1993). The linearity of the stress–strain curves indicates purely elastic deformation of the fibres.

In order to investigate the development of the orientation function during the strain process, single flax fibres were measured in a constant strain rate experiment as stated above. X-ray diffraction images were taken continuously every 2.5 s with 2 s exposures. The X-ray beam was collimated down to 5 µm, thus averaging over a larger area than in the scanning experiment. The sample was not scanned during the experiment.

Fig. 4 shows the orientation function f_c with increasing strain for four different single flax fibres measured at ID13. One fibre (sample flax7) exhibits a significant improvement of f_c during the tensile test. In this case the initial orientation was significantly lower than that in the other measurements. The improvement occurs during the first percent of strain. A stationary value is reached for the remainder of the stretching experiment. For the other three samples a slight tendency towards an improvement of the orientation function is seen; the scatter of the values found decreases with increasing strain. The comparatively low initial value at the beginning of the stretching of sample flax7 cannot be explained by a

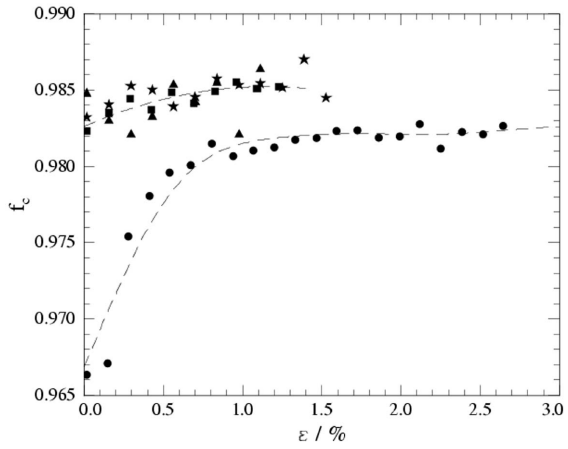

Figure 4
Orientation function f_c for four different single flax fibres with increasing strain, measured at constant strain rate with an X-ray beam of 5 μm in diameter (microfocus beamline ID13, ESRF). Sample flax7 (circles) had a low initial orientation. The dashed lines serve as guide to the eye only.

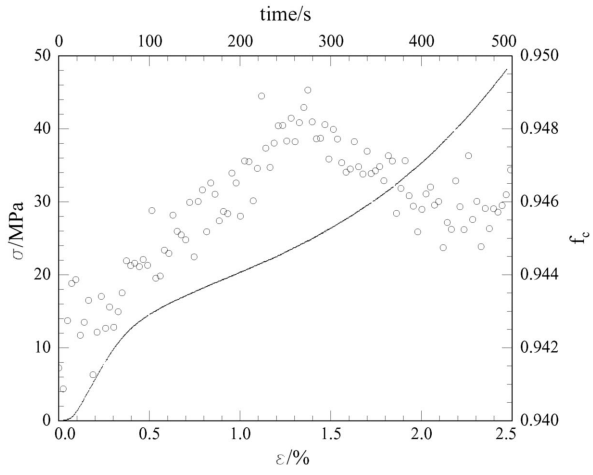

Figure 5
Stress–strain curve of a 0.2 mm × 5 mm × 40 mm section of pine wood (continuous line, left scale) and *in situ* simultaneously measured orientation function f_c of the cellulose microfibrils (circles, right scale). Data were collected with a 250 μm × 250 μm X-ray beam at beamline A2, HASYLAB.

macroscopic orientation effect of a bundle of several fibres, since only an individual fibre was examined. Instead this points to the presence of badly oriented areas within the fibre. The X-ray beam, albeit larger than during the scanning experiments described above, was apparently focused to such a part of the fibre. The interpretation is corroborated by the comparably low Young's modulus of 11.0 GPa of this particular fibre.

In contradiction to our findings, Astley & Donald (2003) claim that in a similar *in situ* X-ray diffraction experiment they did not observe a change of the orientation distribution of a bundle of industrial flax fibres upon uniaxial strain. We briefly re-analysed their azimuthal 200 reflection profiles (Astley & Donald, 2003, Fig. 8) and found a decrease of the reflection widths (FWHM) by about 15% at 1% strain. That effect is of the same order of magnitude as that reported here (at 1% strain: 20% for flax7, 10% for our other samples). The sharpening of the peaks in the azimuthal direction compensates for the increase in peak intensity observed by Astley & Donald (2003). The integrated intensity of the 200 reflection stays constant within the statistical error, ruling out the strain-induced crystallization proposed by Astley & Donald (2003).

3.3. Stretching experiment on spruce wood with constant strain rate (HASYLAB, A2)

The wood samples were measured with a beam of 250 μm × 250 μm, thus averaging over about 100 individual tracheid cells (typical cross section 20 μm × 20 μm) in a 200 μm-thick sample. As in the experiment described in the previous section, stretching was carried out with a constant strain rate in order to avoid relaxation. We chose a rate of 2 μm s^{-1}, corresponding to 0.005% s^{-1} for a 4 cm-long wood foil. The stress–strain curve of a typical sample is shown in Fig. 5 (continuous line). It is linear (elastic) for the first 0.4% with an initial Young's modulus of 3.2 GPa. Beyond the yield point (onset of plastic deformation), the Young's modulus is reduced to 1.0 GPa. At about 1.2% strain, an onset of strain hardening is observed until the wood sample breaks at 2.5% strain (tensile strength 48 MPa).

X-ray diffraction images were taken every 4.5 s with an exposure time of 3 s. Fig. 1 is a typical two-dimensional diffraction diagram. Obviously, the microfibril angle is quite small as the 200 reflections are not split on the azimuth (Keckes *et al.*, 2003). The azimuthal intensity profile is nearly Gaussian, with a width (FWHM) of 19.5°, meaning that the MFA is smaller than $\sigma = 8.3°$ (Lichtenegger *et al.*, 1998), *i.e.* the cellulose microfibrils are well oriented with respect to the longitudinal cell axis. Upon stretching, changes of the azimuthal width of the 200 Bragg reflections are observed. For Fig. 5, Hermans' orientation function f_c (circles) has been calculated from the average of the azimuthal widths of both the left and the right 200 reflections. The most prominent feature of the f_c dependence on strain is a distinct maximum at $\varepsilon = 1.3\%$. Up to this value, the orientation of the cellulose microfibrils is improved. This result can mean a decrease of the MFA, a rotation of the microfibrils leading to a narrower orientation distribution (as in the case of flax, see above) or a combination of the two effects. In all three cases the crystalline microfibrils have to rotate in the soft matrix of the nanocomposite material wood. The change of slope in $f_c(\varepsilon)$ around the yield point of the stress–strain curve needs further proof. At higher strain than 1.3% and until the wood breaks, the microfibril orientation surprisingly degrades again. This unexpected effect coincides with strain hardening of the wood. Further investigation of the microscopic origin of this behaviour is in progress.

4. Conclusions and outlook

The results of tensile tests on cellulose fibres and wood reported here demonstrate the power of synchrotron X-ray diffraction techniques for *in situ* experiments. At second-

generation synchrotron sources the use of modern CCD detectors with image intensifiers and short read-out times enables experiments with constant strain rates. Focused microbeams at third-generation sources can be exploited for high spatial resolution (scanning) or for fast stretching experiments on single microscopic fibres. In all cases shown here, series of two-dimensional diffraction diagrams were obtained, allowing for the determination of structural parameters with high accuracy. With the advent of more powerful detectors in the near future, even the combination of scanning and fast tensile testing will become feasible.

This article focuses on the orientation changes of cellulose microfibrils in flax fibres and wood upon stretching. *In situ* tensile tests on single flax fibres with highly oriented cellulose microfibrils revealed a significant improvement of the microfibril orientation with increasing strain. This result means that the cellulose microfibrils rotate in the softer embedding matrix of this nanocomposite material. We observed that the irregular spatial distribution of more or less ordered regions becomes much more homogeneous. There seems to be a saturation value for Hermans' orientation function f_c of about 0.99, *i.e.* an almost perfect orientation. We measured in two different modes, either waiting for complete relaxation after setting a new strain value or with a constant strain rate faster than relaxation. From the fact that the orientation changes occur more readily at lower strain in the fast stretching experiment we may preliminarily conclude that at up to 1% strain a decrease of orientation is a possible relaxation mechanism. *In situ* relaxation studies are required to corroborate these findings concerning the viscoelastic properties. In order to gain a complete picture of the microscopic and nanoscopic yield mechanisms of native cellulose fibres an analysis of the change of crystalline cellulose lattice constants under stress is planned.

The study of pine wood with low microfibril angle (below 8°) revealed a more complex behaviour of both the stress–strain characteristics (distinct yield point, strain hardening) and the details of the orientation changes of the microfibrils upon stretching observed here for the first time (increase of orientation only up to 1.3%, then again degradation). Future work will concentrate on the microscopic mechanism of plastic deformation and on viscoelastic effects.

The authors thank Ingo Burgert (MPI Golm, Germany), Christoph Czihak (University of Vienna, Austria), Jozef Keckes (University of Leoben, Austria), Christian Riekel (ESRF, Grenoble, France) and Helmut Schober (Institut Laue–Langevin, Grenoble, France) for their help with some of the experiments. Technical support by Lionel Lardière and Jens Meyer (both ESRF) is gratefully acknowledged.

References

Alexander, L. E. (1979). *X-ray Diffraction Methods in Polymer Science*, ch. 4–4. Huntington, NY: Krieger.
Astley, O. M. & Donald, A. M. (2003). *J. Mater. Sci.* **38**, 165–171.
Burghammer, M., Müller, M. & Riekel, C. (2003). *Recent Res. Dev. Macromol.* **7**, 103–125.
Cave, I. D. (1997). *Wood Sci. Technol.* **31**, 143–152, 225–234.
Hammersley, A. P., Svensson, S. O. & Thompson, A. (1994). *Nucl. Instrum. Methods Phys. Res. A*, **346**, 312–321.
Jakob, H. F., Fratzl, P. & Tschegg, S. E. (1994). *J. Struct. Biol.* **113**, 13–22.
Keckes, J., Burgert, I., Frühmann, K., Müller, M., Kölln, K., Hamilton, M., Burghammer, M., Roth, S. V., Stanzl-Tschegg, S. & Fratzl, P. (2003). *Nature Mater.* **2**, 810–814.
Lichtenegger, H., Müller, M., Paris, O., Riekel, C. & Fratzl, P. (1999). *J. Appl. Cryst.* **32**, 1127–1133.
Lichtenegger, H., Reiterer, A., Tschegg, S. & Fratzl, P. (1998). *Microfibril Angle in Wood*, edited by B. G. Butterfield, pp. 140–156. Christchurch, New Zealand: University of Canterbury.
Morton, W. E. & Hearle, J. W. S. (1993). *Physical Properties of Textile Fibers*, 3rd ed. Manchester: The Textile Institute.
Müller, M., Czihak, C., Burghammer, M. & Riekel, C. (2000). *J. Appl. Cryst.* **33**, 817–819.
Müller, M., Czihak, C., Vogl, G., Fratzl, P., Schober, H. & Riekel, C. (1998). *Macromolecules*, **31**, 3953–3957.
Müller, M., Riekel, C., Vuong, R. & Chanzy, H. (2000). *Polymer*, **41**, 2627–2632.
Noack, D. & Schwab, E. (1996). *Holzbau-Taschenbuch. Band 1: Grundlagen, Entwurf und Konstruktionen*, 9th ed., edited by R. von Halasz & C. Scheer, pp. 7–33. Berlin: Ernst and Sohn.
O'Sullivan, A. C. (1997). *Cellulose*, **4**, 173–207.
Reiterer, A., Lichtenegger, H., Tschegg, S. & Fratzl, P. (1999). *Philos. Mag. A*, **79**, 2173–2184.
Riekel, C. (2000). *Rep. Prog. Phys.* **63**, 233–262.
Riekel, C., Dieing, T., Engström, P., Vincze, L., Martin, C. & Mahendrasingham, A. (1999). *Macromolecules*, **32**, 7859–7865.
Satta, A., Hagege, R. & Sotton, M. (1986). *Bull. Sci. ITF*, **15**, 3–13.
Stein, R. S. (1958). *J. Polym. Sci.* **31**, 327–334.
Woodcock, C. & Sarko, A. (1980). *Macromolecules*, **13**, 1183–1187.